Stochastic random network model in Ge and Si chalcogenide glasses

S. Sugai
Department of Physics, Faculty of Science, Osaka University, 1-1 Machikaneyama-cho, Toyonaka, Osaka 560, Japan
(Received 28 April 1986)

A stochastic random network model is proposed for the structure of Ge_xS_{1-x}, Ge_xSe_{1-x}, Si_xS_{1-x}, and Si_xSe_{1-x} ($x \leqq 0.33$) glasses. This model is constructed to explain the existence of two types of microcrystalline states induced by photoirradiation above or below the threshold intensity. This model characterizes the glass structure by one parameter P which is related to the existing probability of the edge-sharing bonds between the tetrahedral MX_4 molecules relative to the corner-sharing bonds. P depends only on the species of atoms forming the glass and not on x. In order to prove the validity of the present model, Raman scattering experiments were made and the x dependence of the intensity ratio of the A_1^c companion peak to the A_1 peak, $I(A_1^c)/I(A_1)$, was obtained. From the viewpoint of phonon localization, the A_1 mode is assigned to the breathing mode of MX_4 molecules and the A_1^c mode to the vibration of chalcogen atoms on the edge-sharing double bonds. The x dependence of the intensity ratio $I(A_1^c)/I(A_1)$ calculated by the present model is in good agreement with the experimentally obtained ratio. The P obtained increases in order from Ge_xS_{1-x}, Ge_xSe_{1-x}, Si_xSe_{1-x} to Si_xS_{1-x} with the same order of tendency of getting edge-sharing bonds in the crystals. The value of P is independent of the method of making the amorphous but it can be changed by photoirradiation. P decreases with irradiation below the threshold intensity, but it increases with irradiation above the threshold. The local energy in the glass is lower in the corner-sharing bonds, but the total energy is lowest in the same structure as the crystal. The threshold irradiation intensity for Se glass is less than one-hundredth of that for $GeSe_2$ glass.

I. INTRODUCTION

Intensive experiments on the lattice vibrations have been done in typical glassy semiconductors Ge_xSe_{1-x},[1-15] Ge_xS_{1-x},[16-20] Si_xSe_{1-x},[21-27] and Si_xS_{1-x}.[21,23,28] The assignment of the Raman peaks and the resulting glassy structures is, however, still controversial. The characteristic feature in the Raman spectra of $GeSe_2$ glass is the appearance of two large A_1 peaks at 201 and 217 cm^{-1} in place of a large single A_g peak at 211 cm^{-1} in the crystal. The peak at 217 cm^{-1} in the $GeSe_2$ glass is called the companion A_1^c peak. The intensity ratio of the A_1^c peak to the A_1 peak, $I(A_1^c)/I(A_1)$, changes drastically with the Ge concentration in Ge_xSe_{1-x} glasses.[1]

Before the proposal of the "outrigger-raft" model[6] (ORM), the chemically ordered random-network model (RNM) had been generally accepted in $x \leqq 0.33$, but trials to explain the x dependence of the intensity ratio $I(A_1^c)/I(A_1)$ by small molecular units have yielded unsatisfactory results.[1,2] It is generally accepted that the A_1 peak is due to the breathing vibrational mode of methane-like $GeSe_{4/2}$ molecules, but the origin of the A_1^c peak has been controversial. Bridenbaugh *et al.*[6] tried to explain the A_1^c peak by the structure which does not exist in the crystal, and proposed the ORM for the glass structure of $GeSe_2$. In this model the $GeSe_2$ glass is composed of wide bands which have the same structure as the crystal inside the band, but are terminated by Se—Se bonds at both sides. This model stresses the similarity between the glass and the crystal.

I found, however, that there exist two different kinds of photoinduced microcrystalline states.[29] The two distinct microcrystalline phases are produced according to the intensity of irradiated light and not the accumulated intensity of light. This two-directional microcrystallization is more favorable for the RNM than for the ORM, because the former model has equal opportunity for the structural change to the different microcrystalline phases, but the latter model has only one possibility for the crystallization.

The purpose of the present paper is to show the validity of the RNM. The A_1^c mode is assigned from the viewpoint of phonon localization to the vibration of chalcogen atoms on the edge-sharing bonds. This assignment is consistent with the suggestion by Nemanich *et al.*[30] and Lucovsky *et al.*[31] Based on this assignment a stochastic RNM is proposed for the glass structure. This model has only one parameter P which depends on only the species of atoms forming the glass and does not depend on x. It is shown that this model gives the x dependence of the intensity ratio, $I(A_1^c)/I(A_1)$, in good accordance with the experimental results.

For the purpose of getting the exact ratio $I(A_1^c)/I(A_1)$ Raman scattering experiments were done on Ge_xS_{1-x}, Ge_xSe_{1-x}, Si_xS_{1-x}, and Si_xSe_{1-x} ($x \leqq 0.33$). In the experiment of photoinduced crystallization of glassy $GeSe_2$ and $SiSe_2$, it is found that P can be changed by the photoirradiation.

The interpretation of Raman spectra from the viewpoint of localized phonons is presented in Sec. II. Experimental results of Raman scattering and the Gaussian decomposition of the spectra are given in Sec. III.

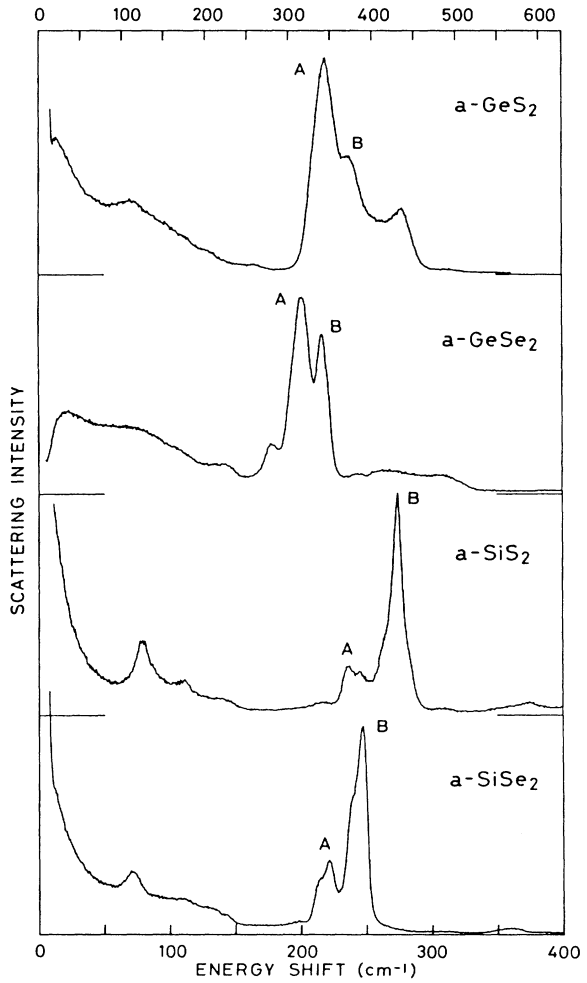

FIG. 1. The Raman spectra in GeS_2, $GeSe_2$, SiS_2, and $SiSe_2$ glasses. The lower energy scale is for selenides and the upper is for sulfides. The upper scale is contracted by $(M_S/M_{Se})^{1/2}$.

TABLE I. The chemical reaction temperatures (°C) before the water quenching.

x	Ge_xSe_{1-x}	Ge_xS_{1-x}	Si_xSe_{1-x}	Si_xS_{1-x}
0.33	900	950	1060	1050
0.3	900	900	1010	(1050)[a]
0.25	900	830	1010	(1000)[b]
0.2	900	830	1010	(1000)[b]
0.15	900	830	1000	
0.1	900	830	1000	
0.05	900	830	1000	
0	900	830	1000	

[a]Phase-separated nonuniform glass.
[b]Explosion on raising temperature.

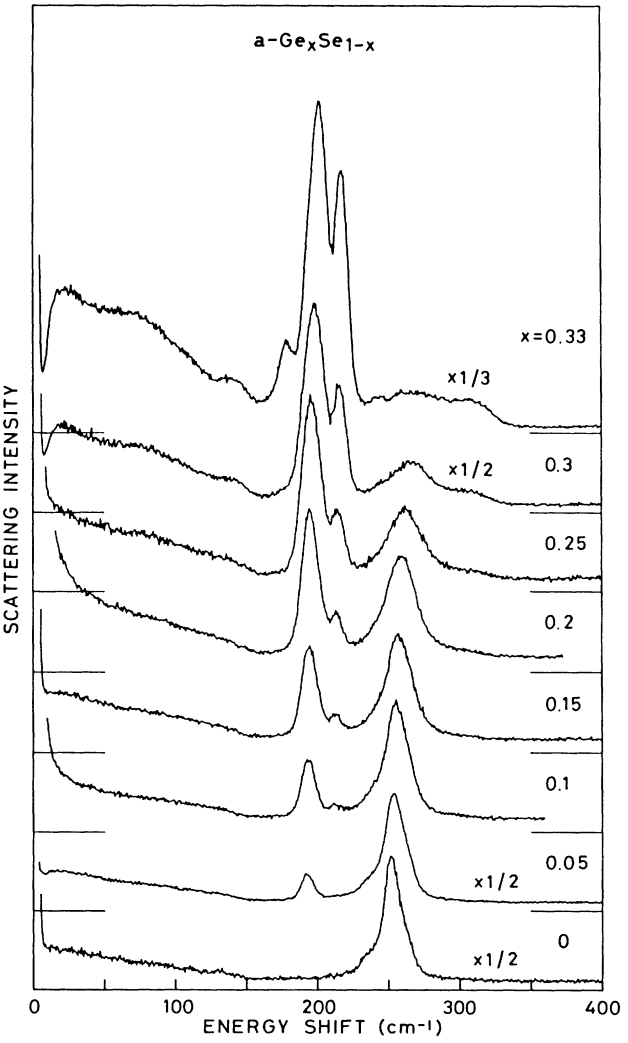

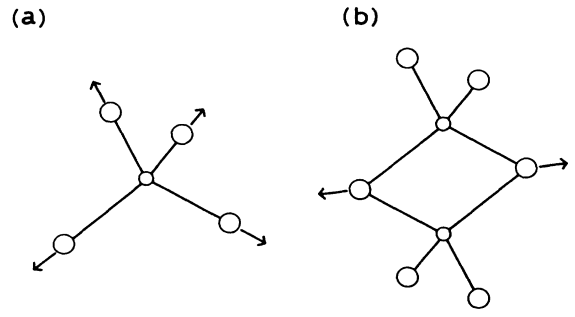

FIG. 2. The A_1 modes in the corner-sharing tetrahedron (a) and in the edge-sharing tetrahedron (b).

FIG. 3. The Raman spectra in Ge_xSe_{1-x} ($x \leqq 0.33$) glasses.

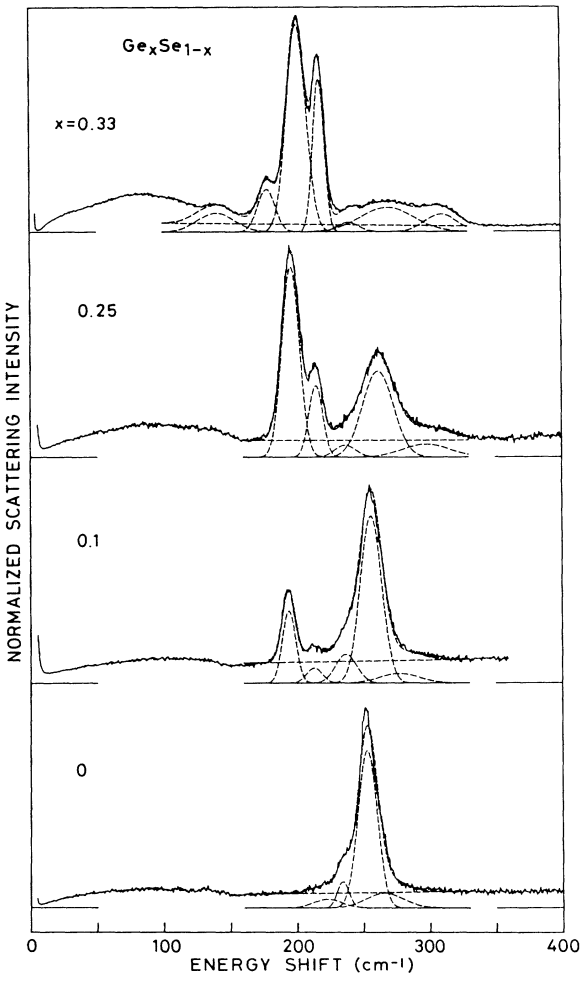

FIG. 4. The Raman spectra in Ge_xSe_{1-x} glasses and their decomposed Gaussian curves. The intensity is normalized by the statistical factor.

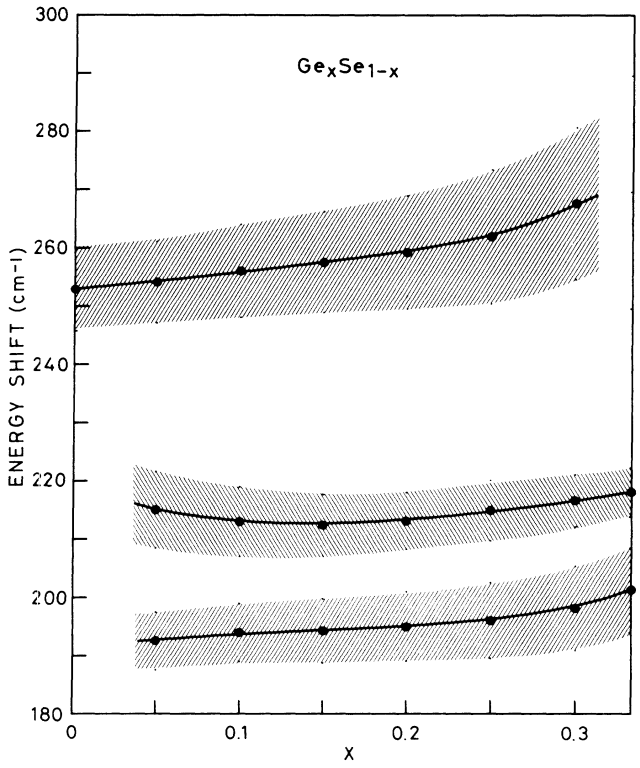

FIG. 5. The x dependence of the A_1 and A_1^c modes in the $GeSe_4$ tetrahedra and the A_1 mode in the Se_8 rings. The edges of the screen tones show the energies of $\omega_j \pm \sigma_j$.

The stochastic random network model is presented in Sec. IV. It is shown that this model reproduces the intensity ratio $I(A_1^c)/I(A_1)$ in good accordance with the experimental results. The change of the parameter P in the course of photoinduced crystallization is demonstrated in Sec. V. The origin of the low-frequency peak and other problems are discussed in Sec. VI.

II. INTERPRETATION OF THE RAMAN SPECTRA FROM THE VIEWPOINT OF PHONON LOCALIZATION

Most of the analyses of lattice vibrations in glasses have been done by analogy with the crystals. In those analyses the main difference from the crystal is the lack of momentum conservation. The spectra in glasses are interpreted as the phonon density of states in the crystals. Bridenbaugh *et al.*[6,32] compared the Raman spectra in the glassy $GeSe_2$ with those from the Γ-point modes in the crystal. They assigned the 210 cm^{-1} mode in the crystal and the 198 cm^{-1} mode in the glass to the A_1 mode in the corner-sharing $GeSe_{4/2}$ tetrahedra, and the companion mode at 215 cm^{-1} in the crystal to the A_1 mode in the edge-sharing tetrahedra. The origin of the companion peak at 212 cm^{-1} in the glass was the problem. The energy difference 14 cm^{-1} between the A_1 and its companion modes in the glass is much larger than the difference 5 cm^{-1} in the crystal. The relative scattering intensity of

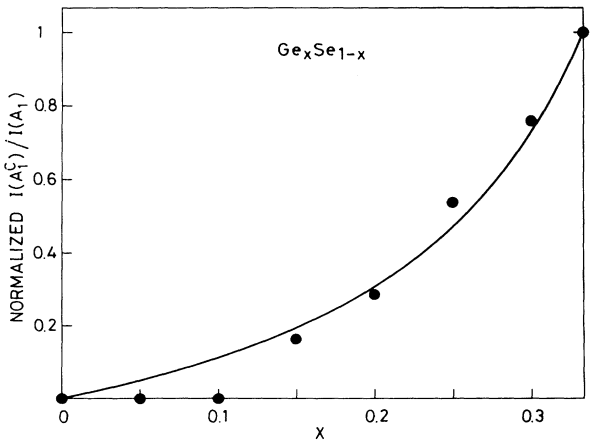

FIG. 6. The intensity ratio $I(A_1^c)/I(A_1)$ normalized at $x=0.33$. The curve is calculated by the stochastic random network model presented in the text.

TABLE II. The phonon energies, scattering intensities normalized by the A_1 peak intensity, and the standard deviations of the energies in Ge_xSe_{1-x}, Ge_xS_{1-x}, Si_xSe_{1-x}, and Si_xS_{1-x} glasses obtained from the Gaussian fitting. The A_1 mode is denoted by A and the A_1^c by C.

	Ge_xSe_{1-x}				Ge_xS_{1-x}				Si_xSe_{1-x}				Si_xS_{1-x}			
x	Mode	ω (cm^{-1})	I	σ (cm^{-1})	Mode	ω (cm^{-1})	I	σ (cm^{-1})	Mode	ω (cm^{-1})	I	σ (cm^{-1})	Mode	ω (cm^{-1})	I	σ (cm^{-1})
0.33		140.4	0.17	13.9	A	342.9	1.00	13.1		200.5	0.08	6.9		340.0	0.21	14.0
		178.5	0.18	6.5	C	374.2	0.26	9.6	A	212.5	0.24	3.2	A	368.6	0.26	5.3
	A	201.2	1.00	7.3		400.1	0.55	26.1	A	221.6	0.76	4.7	A	383.4	0.74	11.1
	C	218.0	0.43	4.2		437.3	0.18	10.4	C	240.4	1.86	5.4	C	426.7	2.78	14.2
		240.0	0.05	8.0		481.5	0.01	15.2	C	248.0	1.19	3.0	C	430.3	0.87	4.1
		269.5	0.32	20.0										486.0	0.10	10.0
		310.0	0.14	12.0												
0.3		178.0	0.03	6.5	A	341.1	1.00	10.8	A	210.1	0.18	3.7				
	A	198.2	1.00	7.2	C	370.0	0.24	10.6	A	218.4	0.82	5.0				
	C	216.6	0.36	4.5		399.0	0.54	28.0	C	236.7	0.67	3.8				
		244.0	0.08	10.0		437.2	0.09	8.9	C	244.0	0.67	3.8				
		267.5	0.42	13.0		481.1	0.10	15.0		260.3	0.39	5.7				
		306.0	0.14	13.0						273.3	1.12	6.3				
0.25	A	196.1	1.00	6.5	A	341.0	1.00	10.1	A	207.7	0.12	4.0				
	C	214.9	0.30	5.2	C	368.2	0.21	10.7	A	216.2	0.88	5.9				
		237.0	0.08	8.0		396.4	0.63	31.0	C	240.0	0.94	6.0				
		261.9	0.79	11.5		437.7	0.06	8.0		266.0	3.74	9.5				
		298.0	0.19	18.0		476.9	0.16	13.3								
0.2	A	195.0	1.00	6.0	A	342.0	1.00	9.0	A	213.9	1.00	6.4				
	C	213.1	0.22	4.9	C	368.0	0.18	10.0	C	237.6	1.08	5.9				
		237.5	0.21	10.0		398.0	0.69	31.0		261.3	6.72	9.5				
		259.2	1.25	9.7		437.5	0.07	7.7								
		284.7	0.27	17.9		470.1	0.44	12.0								
						477.0	0.07	3.6								
0.15	A	194.3	1.00	5.5	A	343.2	1.00	9.1	A	213.4	1.00	6.3				
	C	212.4	0.23	5.3	C	368.0	0.15	9.2	C	236.2	1.43	6.2				
		236.2	0.33	9.1		398.0	0.68	30.0		258.7	10.49	8.9				
		257.5	1.92	8.7		436.5	0.12	8.3		266.5	0.96	19.3				
		275.7	0.40	17.8		470.0	0.73	12.0								
						476.0	0.15	3.4								
0.1	A	194.0	1.00	5.0	A	343.5	1.00	8.0	A	213.4	1.00	7.7				
	C	213.0	0.25	6.0	C	367.5	0.14	9.0	C	234.6	1.64	5.9				
		237.0	0.64	8.0		400.0	0.93	35.0		255.5	12.33	8.0				
		256.0	3.70	8.0		433.0	0.11	6.0		263.2	2.15	16.3				
		277.0	0.40	15.0		444.0	0.10	5.0								
						471.0	1.25	10.5								
						475.5	0.44	3.4								

TABLE II. (*Continued*).

	Ge_xSe_{1-x}				Ge_xS_{1-x}				Si_xSe_{1-x}				Si_xS_{1-x}			
x	Mode	ω (cm^{-1})	I	σ (cm^{-1})	Mode	ω (cm^{-1})	I	σ (cm^{-1})	Mode	ω (cm^{-1})	I	σ (cm^{-1})	Mode	ω (cm^{-1})	I	σ (cm^{-1})
0.05	A	192.6	1.00	5.0	A	343.7	1.00	8.1	A	212.8	1.00	6.0				
	C	215.0	0.26	6.6	C	367.9	0.09	8.5	C	234.4	2.16	7.0				
		235.9	1.33	7.0		401.8	1.08	39.3		255.3	8.68	6.0				
		254.1	6.78	7.0		431.9	0.24	5.9		256.9	13.94	11.0				
		270.2	0.89	14.6		443.0	0.30	5.1								
						472.0	2.30	9.9								
						475.5	1.61	3.4								
0		222.3	0.06	10.6		414.8	0.03	9.0		222.0	0.05	10.0				
		234.3	0.08	4.4		432.1	0.08	6.0		234.0	0.08	5.2				
		252.8	0.73	7.2		442.0	0.06	4.9		251.3	0.30	4.7				
		265.5	0.13	14.1		470.8	0.40	11.0		254.8	0.57	9.7				
						474.0	0.43	3.5								

the companion peak in the crystal is much smaller than in the glass. From those facts they concluded that the companion mode in the glass is different from the edge-sharing mode as in the crystal. They proposed the ORM to give the structure which does not exist in the crystal and assigned the A_1^c mode to the vibration of dimerized Se atoms at the edges of the outrigger-raft clusters.

I, however, propose to assign the A_1 and the A_1^c peaks in the glass to the localized modes at the corner-sharing bonds and the edge-sharing bonds, respectively. These bonding forms exist even in the crystal, but the phonon energy in the crystal is quite different from both energies of the A_1 and A_1^c modes in the glass, because the energy of the nonlocalized mode in the crystal is not the pure A_1 mode at the corner-sharing bonds nor that at the edge-sharing bonds. The energies and the eigenvectors of the crystalline modes are determined by solving the characteristic equation including the interaction between the A_1 and the A_1^c modes.

Very recently Akkermans and Maynard[33] presented the theory of phonon localization in disordered materials by the use of analogy with the Anderson localization of electrons. The theory uses the mass defect model in the weak localization regime. The theory elucidates the existence of a threshold frequency for the localization of phonon density fluctuation. The threshold frequency is expressed by $\omega_3^*=0.51\sigma_M^{-2/3}\omega_D$ in the three-dimensional case, where σ_M^2 is the local fluctuation of mass and ω_D is the Debye frequency. For the extreme case of disorder $\sigma_M \sim 1$ and ω_3^* is less, but not far from ω_D. The theory shows the enhancement of the one-phonon spectral density and the shortening of the one-phonon mean lifetime in the vicinity of ω_3^* via the anharmonic interphonon interaction. It is suggested that the localization of the acoustic phonon density at ω_3^* could explain the origin of existence of a plateau at around 10 K in thermal conductivity accompanied by excess specific heat in all glasses.

The Raman spectra in glassy GeS_2, $GeSe_2$, SiS_2, and $SiSe_2$ are shown in Fig. 1. All of these spectra have the A_1 and A_1^c peaks in spite of the variety of their crystal structures, although the intensity ratio depends on the material. The crystal structures of these compounds are composed of methane-like $MX_{4/2}$ molecules. The difference in the materials is how the molecules are bonded. Two kinds of bonding forms, the corner-sharing single bond and the edge-sharing double bond, are known for the bonding between two molecules. These are shown in Fig. 2. The low-temperature phase of GeS_2 is a three-dimensional structure composed of only corner-sharing bonds.[34] $GeSe_2$ (Ref. 35) and the high-temperature phase of GeS_2 (Ref. 36) are two dimensional and composed of two kinds of bonds. SiS_2 and $SiSe_2$ crystallize in one-dimensional structures which have only edge-sharing bonds.[37]

In the present analysis of Raman spectra in Ge and Si chalcogenide glasses we suppose that the A_1 and the A_1^c modes in these glasses are in the localization limit, and the vibrational frequency is determined only by the molecular units. The A_1 mode is assigned to the breathing mode in the methane-like molecule joined by the corner-sharing bonds and the A_1^c mode to the vibration of chal-

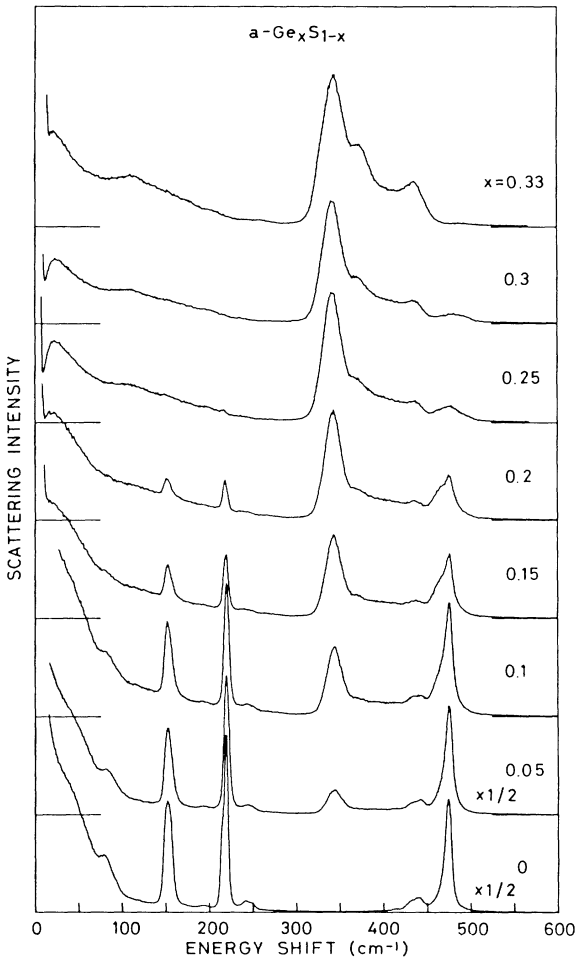

FIG. 7. The Raman spectra in Ge_xS_{1-x} ($x \leqq 0.33$) glasses.

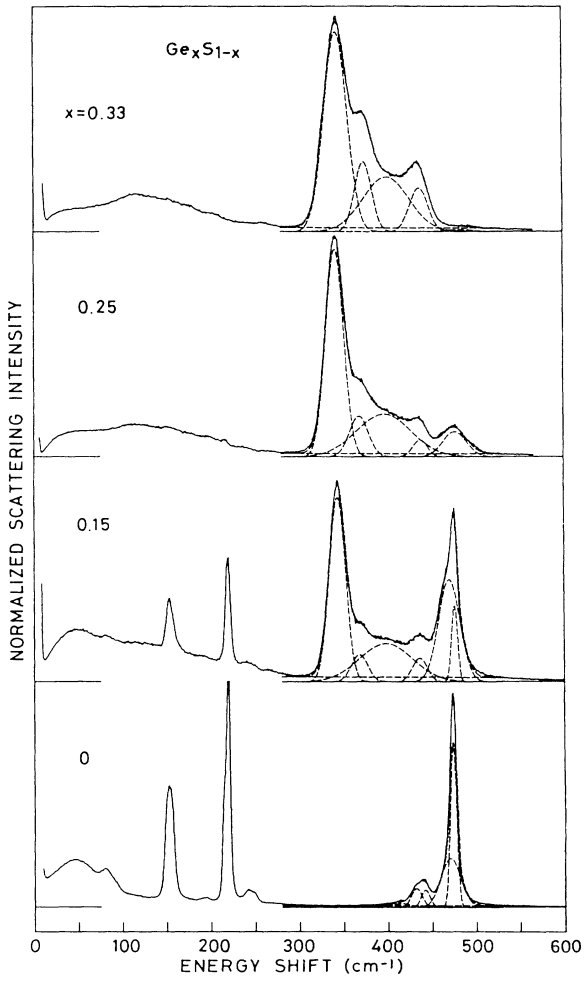

FIG. 8. The Raman spectra in Ge_xS_{1-x} glasses and their decomposed Gaussian curves. The intensity is normalized by the statistical factor.

cogen atoms on the double bond as shown by the arrows in Fig. 2. The higher energy of the vibrational mode in the edge-sharing bonds than in the corner-sharing bonds is expected from the shorter interatomic distance between chalcogen atoms on the double bond than twice the van der Waals radius.[35] This assignment is supported from the fact that the A_1 peak energy in glassy GeS_2 is the same as the energy of the largest A_g peak in the low-temperature phase of crystalline GeS_2,[20] and the A_1^c peak energies in SiS_2 and $SiSe_2$ glasses are almost the same as the A_g peak energies in their crystals.[21,22,24,25] These crystals consist of a single type of molecular bonds. In the crystals of $GeSe_2$ and the high-temperature phase of GeS_2 the A_g modes with the largest scattering intensity are assigned to the in-phase vibrational modes among both types of molecules shown in Fig. 2.

Calculation of the phonon density of states in glassy $GeSe_2$ were done by Murase *et al.*[38] and Aronovitz *et al.*[39] Those calculations aimed to give the evidence of the origin of the companion peak on the basis of the ORM. But they did not succeed in obtaining the companion peak directly. Lucovsky *et al.*[31] calculated the vibrational spectra of the $GeSe_2$ Bethe lattice using a random dihedral-angle distribution and showed that all the spectral features can be accounted for except the companion peak. They assigned the companion peak to the mode of Fig. 2(b).

III. RAMAN SPECTRA AND THEIR GAUSSIAN DECOMPOSITION

Samples of Ge and Si chalcogenide glasses were made by quenching into water, after keeping them melted for one to several days. The temperatures from which the samples were quenched are listed in Table I. The sample of Si_xS_{1-x} with $x \leqq 0.3$ obtained by quenching from the temperature below 950 °C shows clear two-phase separation. The sample of $Si_{0.3}S_{0.7}$ obtained from 1050 °C looks uniform, but the Raman spectra are simply the sum of SiS_2 and S glasses. On increasing temperature to 1000 °C the quartz ampoules containing Si_xS_{1-x} with $x \leqq 0.25$ exploded.

Raman scattering experiments were made in a back-scattering configuration at room temperature. A 6328 Å He-Ne laser was used for selenide glasses and a 5145 Å Ar-ion laser for sulfide glasses. The Ar-ion laser was operated at 4579 Å in the experiments of photoinduced crystallization of $SiSe_2$ glass. The samples were kept in quartz ampoules which were used in the synthesis process. For the experiments of Raman scattering, except for the photoinduced crystallization, a cylindrical lens was used in order to reduce the photon density. The incident light was weakened by neutral density filters for Se-rich samples of $x<0.1$, because they crystallize very easily by the laser beam. In sulfide glasses the crystallization becomes very easy even in the dark at room temperature, on approaching pure sulfer. The sample changes from transparent yellow to milky yellow within several minutes or several tens of minutes after quenching into ice water. Most of Raman data were obtained from the transparent areas.

Figure 3 shows the concentration dependence of Raman spectra in Ge_xSe_{1-x} glasses ($0 \leqq x \leqq 0.33$). These spectra are consistent with the reported data.[1-3,5,7] In order to obtain the peak energy, width, and relative scattering intensity exactly, the normalized spectra by the Bose occupation factor are decomposed into a set of Gaussian peaks as

$$I_{\text{normalized}}(\omega)=I_{\text{obs}}(\omega)/[n(\omega,T)+1]=\sum_j I_j(2\pi\sigma_j^2)^{-1/2}\exp[-(\omega-\omega_j)^2/2\sigma_j^2] .$$

Most of the calculations are made by the least-squares method. Some of the spectra for which the calculations cannot give convergent results are decomposed by comparing the spectra with the sum of Gaussian peaks on a microcomputer screen. The obtained fitting parameters are listed in Table II. The typical results of fitting are shown in Fig. 4. The energies of the A_1 and A_1^c modes in the $GeSe_{4/2}$ tetrahedra and the A_1 mode in the Se_8 rings[40] are shown in Fig. 5 as a function of x. The edges of the screen tones show the energies of $\omega_j \pm \sigma_j$. The x dependence of the relative intensity of the companion peak to the A_1 peak, $I(A_1^c)/I(A_1)$, are plotted in Fig. 6. The $I(A_1^c,x)$ was estimated by

$$I(A_1^c,x)=I_G(A_1^c,x)-\frac{I_G(222\ \text{cm}^{-1},x=0)I_G(236\text{–}270\ \text{cm}^{-1},x)}{I_G(234\ \text{cm}^{-1},x=0)+I_G(253\ \text{cm}^{-1},x=0)} ,$$

to eliminate the scattering component from the pure Se glass, where I_G is the scattering intensity obtained from the Gaussian fit. The x dependence is gentler than the reported results,[1,2] because the linewidth increases with the decrease of x as listed in Table II. These ratios are compared with the calculated values from the stochastic RNM which is presented in the next section.

Figure 7 shows the Raman spectra in Ge_xS_{1-x} glasses. The best fitting parameters for the Gaussian decomposi-

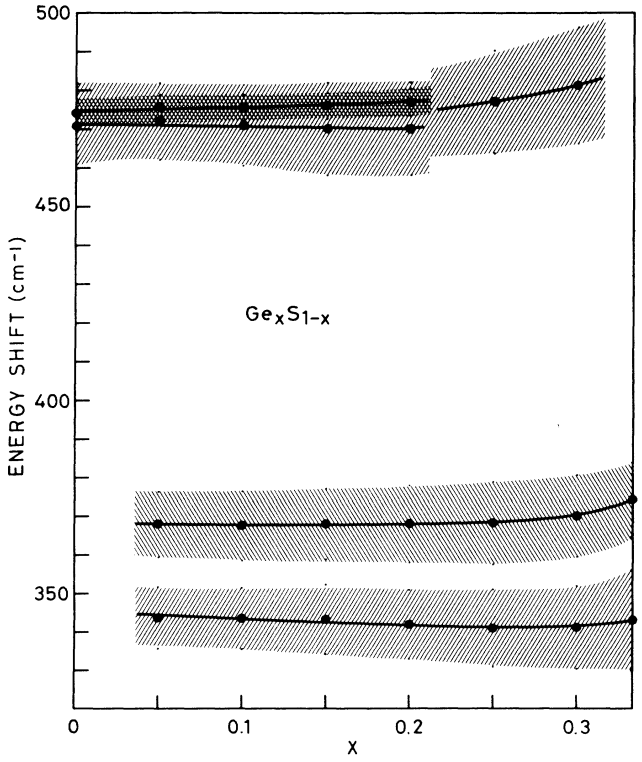

FIG. 9. The x dependence of the A_1 and A_1^c modes in the GeS_4 tetrahedra and the A_1 mode in the S_8 rings. The edges of the screen tones show the energies of $\omega_j \pm \sigma_j$.

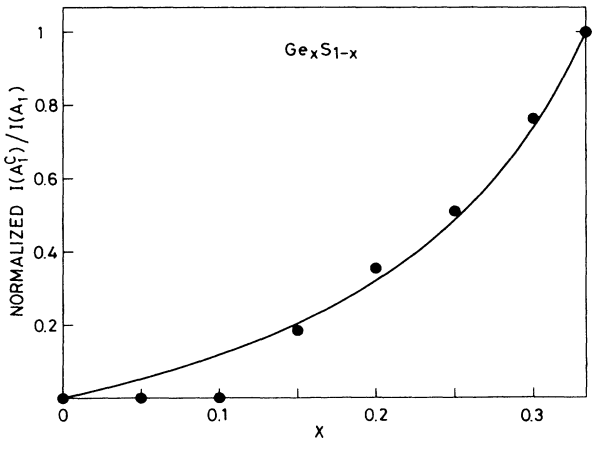

FIG. 10. The intensity ratio $I(A_1^c)/I(A_1)$ normalized at $x=0.33$. The curve is calculated by the stochastic RNM presented in the text.

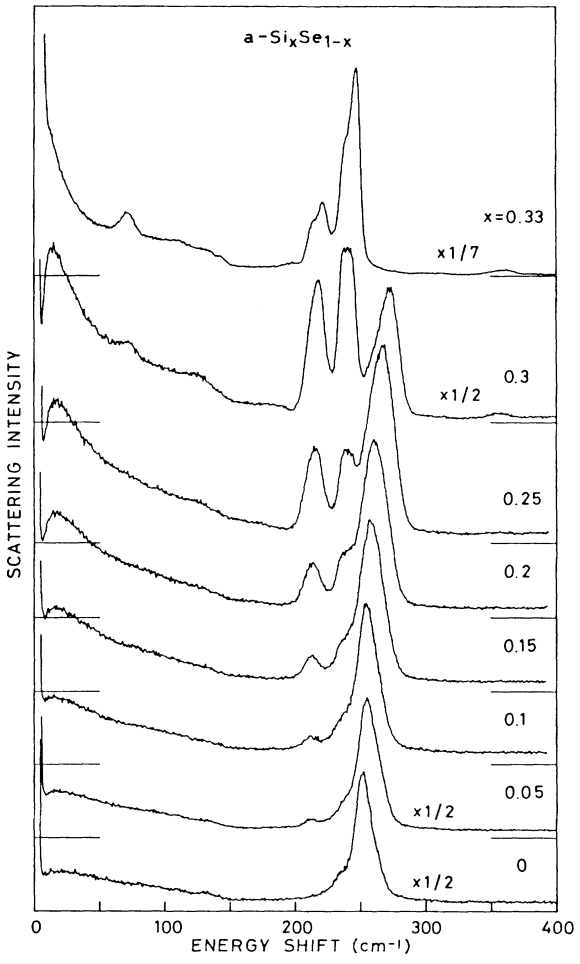

FIG. 11. The Raman spectra in Si_xSe_{1-x} ($x \leq 0.33$) glasses.

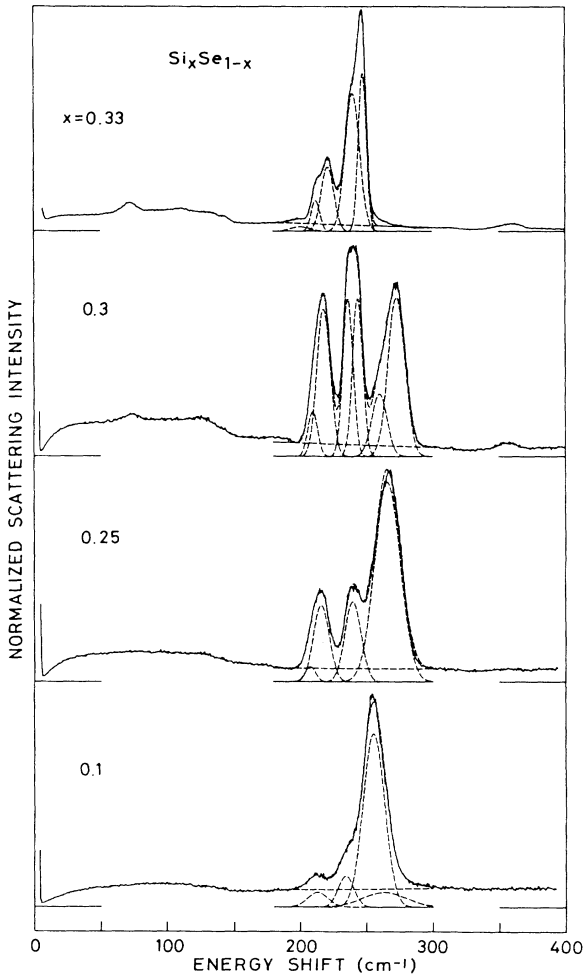

FIG. 12. The Raman spectra in Si_xSe_{1-x} glasses and their decomposed Gaussian curves. The intensity is normalized by the statistical factor.

tion are listed in Table II, and the typical results are shown in Fig. 8. The peak energies of the A_1 and A_1^c modes in the $GeS_{4/2}$ tetrahedra and the A_1 mode in the S_8 rings[41] are shown in Fig. 9. The intensity ratio $I(A_1^c)/I(A_1)$ is shown in Fig. 10. The $I(A_1^c)$ was estimated by

$$I(A_1^c,x)=I_G(A_1^c,x)-0.16I_G(396\text{—}402\ \text{cm}^{-1},x)\ ,$$

to eliminate the intensity overestimated at the Gaussian fit.

Figure 11 shows the Raman spectra of Si_xSe_{1-x} glasses. The fitting parameters are listed in Table II, and the typical fitting curves are shown in Fig. 12. Figure 13 shows the peak energies of the A_1 and A_1^c modes in the $SiSe_{4/2}$ and the A_1 mode in Se_8 rings.[40] The intensity ratio $I(A_1^c)/I(A_1)$ is shown in Fig. 14. The $I(A_1^c)$ was estimated by

$$I(A_1^c,x)=I_G(A_1^c,x)-\frac{I_G(234\ \text{cm}^{-1},x=0)I_G(255\text{—}273\ \text{cm}^{-1},x)}{I_G(251\ \text{cm}^{-1},x=0)+I_G(255\ \text{cm}^{-1},x=0)}\ .$$

The ratio decreases very rapidly on decreasing x from 0.33.

The Raman spectrum in glassy SiS_2 is shown in Fig. 1. The spectra of the Si_xS_{1-x} glasses with nominal concentration $x<0.3$ are only the sum of the spectra from SiS_2 and sulfur glasses. Those glasses are only a mixture of phase-separated SiS_2 glass and sulfur glass. The data of Gaussian fitting of SiS_2 glass are listed in Table II and the decomposed curves are shown in Fig. 15. The intensity ratio, $I(A_1^c)/I(A_1)$, is 3.65.

IV. STOCHASTIC RNM

The photoinduced structural change into two distinct microcrystalline phases is favorable to the RNM because this model has an equal opportunity for the crystallization into two different structures. In RNM all the Ge and Si chalcogenide glasses consist of a random network of methane-like $MX_{4/2}$ molecules. The only difference among the materials is the constitutional ratio between the corner-sharing bonds and the edge-sharing bonds.

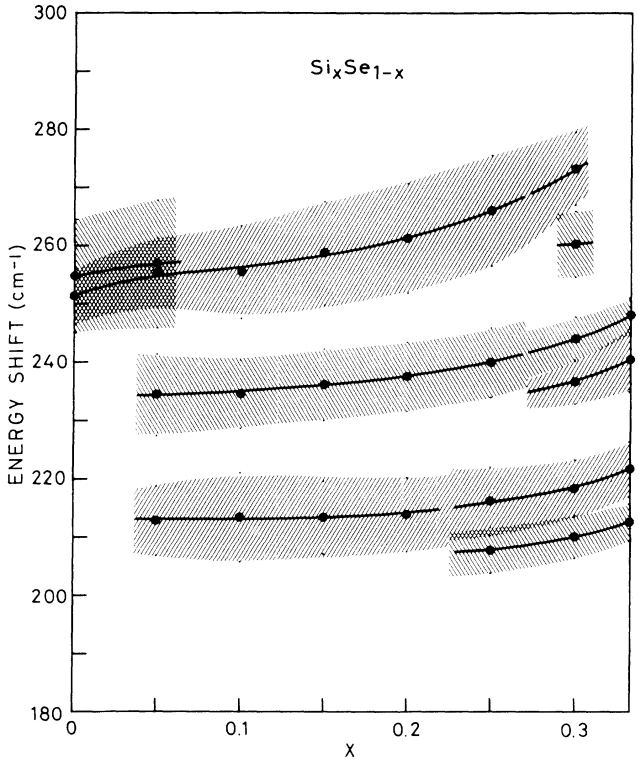

FIG. 13. The x dependence of the A_1 and A_1^c modes in $SiSe_4$ tetrahedra and the A_1 mode in the Se_8 rings. The edges of the screen tones show the energies of $\omega_j \pm \sigma_j$.

Let's imagine adding an atom M on an MX_4 molecule. After the atom M is attached to the MX_4 molecule by a single bond, the probability that the second bond is formed with the atom X which remains unbound in the first MX_4 molecule is supposed to be P times the probability that the second bond is not formed with the first MX_4 molecule. In the case of M_xX_{1-x}, which is written

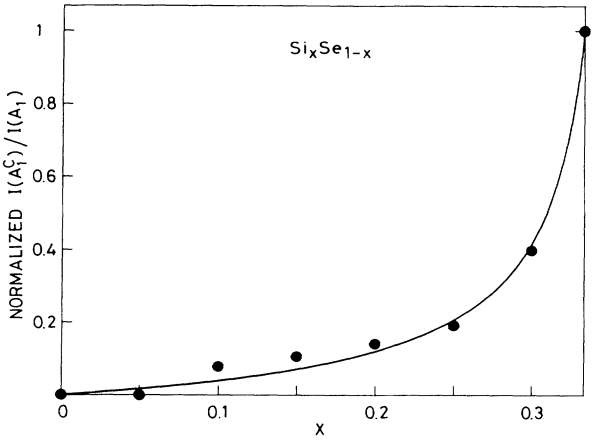

FIG. 14. The intensity ratio $I(A_1^c)/I(A_1)$ normalized at $x=0.33$. The curve is calculated by the stochastic RNM presented in the text.

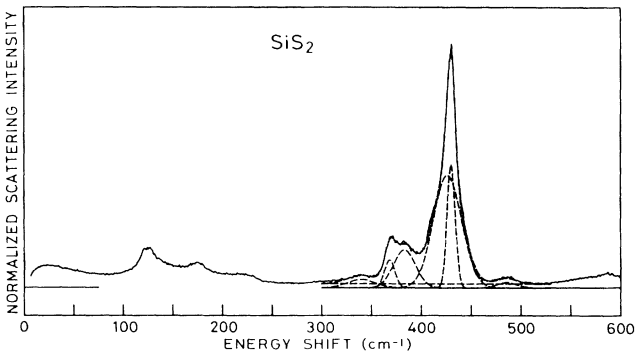

FIG. 15. The Raman spectra in SiS_2 glass.

as $(MX_2)_xX_{1-3x}$, the probability that an X atom of a molecule MX_4 joins to an M atom is $P_M = x/(1-2x)$, and the probability to an X atom is $P_X = (1-3x)/(1-2x)$.

Figure 16 shows all the possible forms of bonding around an MX_4 molecule. The existing probability for each figure is listed in Table III. As for the central MX_4 molecule, the bonding forms in Figs. 16(a)—16(e) consist of X—X bonds and corner-sharing bonds, the forms 16(f)—16(h) X—X, corner-sharing, and edge-sharing bonds, and the form 16(i) only edge-sharing bonds. It is supposed that the X atoms of the MX_4 molecule on the X—X bonds and those on the corner-sharing bonds give almost the same vibrational frequency. We tentatively suppose that the Raman intensity is simply proportional to the number of X atoms which belong to the modes in Figs. 2(a) and 2(b) although the Raman scattering probability is generally different between them. Each of the bonding forms of Figs. 16(a)—16(e) contributes two to the Fig. 2(a) type, each of the forms of Figs. 16(f)—16(h) contributes one to each of the Fig. 2(a) and 2(b) types, and the form of Fig. 16(i) contributes two to the Fig. 2(b) type. The calculated intensity ratio $I(A_1^c)/I(A_1)$ at $x=0.33$ is shown in Fig. 17 as a function of P. The ratio increases monotonically with P. The x dependence of the ratio is shown in Fig. 18 for $P=0.1$, 1, and 5. The decrease of the intensity ratio, on decreasing x from $x=0.33$, becomes drastic with the increase of P.

The best fits for the x dependence of the ratio

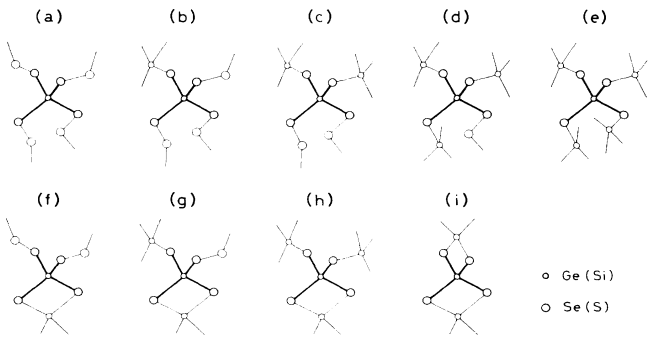

FIG. 16. The possible bonding forms around a tetrahedral MX_4 molecule.

TABLE III. The existing probability for the bonding forms shown in Fig. 16.

Bonding form	Probability
(a)	P_S^4
(b)	$P_S^3 P_G \left[1+\frac{1}{1+P}+\frac{1}{(1+P)^2}+\frac{1}{(1+P)^3}\right]$
(c)	$P_S^2 P_G^2 \left[\frac{1}{1+P}+\frac{1}{(1+P)^2}+\frac{1}{(1+P)(1+2P)}+\frac{1}{(1+P)^3}+\frac{1}{(1+P)^2(1+2P)}+\frac{1}{(1+P)(1+2P)^2}\right]$
(d)	$P_S P_G^3 \left[\frac{1}{(1+P)(1+2P)}+\frac{1}{(1+P)^2(1+2P)}+\frac{1}{(1+P)(1+2P)^2}+\frac{1}{(1+P)(1+2P)(1+3P)}\right]$
(e)	$P_G^4 \frac{1}{(1+P)(1+2P)(1+3P)}$
(f)	$P_S^2 P_G P \left[\frac{3}{1+P}+\frac{2}{(1+P)^2}+\frac{1}{(1+P)^3}\right]$
(g)	$P_S P_G^2 P \left[\frac{2}{1+P}+\frac{2}{(1+P)^2}+\frac{2}{(1+P)(1+2P)}+\frac{6}{(1+P)^2(1+2P)}\right]$
(h)	$P_G^3 P \left[\frac{1}{(1+P)^2}+\frac{2}{(1+P)^2(1+2P)}+\frac{3}{(1+P)(1+2P)(1+3P)}\right]$
(i)	$P_G^2 P^2 \left[\frac{1}{(1+P)^2}+\frac{2}{(1+P)^2(1+2P)}\right]$

TABLE IV. Comparison of P between crystals and glasses. n(ES)/n(CS) is the ratio of the number of chalcogenide atoms on the edge-sharing double bonds to those on the corner-sharing single bonds. P' is estimated from the n(ES)/n(CS), P from the x dependence of the $I(A_1^c)/I(A_1)$ and P^* from the $I(A_1^c)/I(A_1)$ at $x=0.33$ with the assumption of the equal scattering probability between the edge-sharing and the corner-sharing bonds. 3D indicates three-dimensional, 2D two-dimensional, and 1D one-dimensional.

	Structure	GeS_2 3D-LT GeS_2	GeS_2 2D-HT GeS_2	$GeSe_2$ 2D-HT GeS_2	$SiSe_2$ 1D SiS_2	SiS_2 1D SiS_2
Crystal	n(ES)/n(CS)	0	$\frac{1}{3}$	$\frac{1}{3}$	∞	∞
	P'	0	0.12	0.12	∞	∞
Glass	P	0.07		0.15	2.2	
	P^*	0.07		0.15	1.4	1.7
	$I(A_1^c)/I(A_1)$	0.21		0.40	3.1	3.7

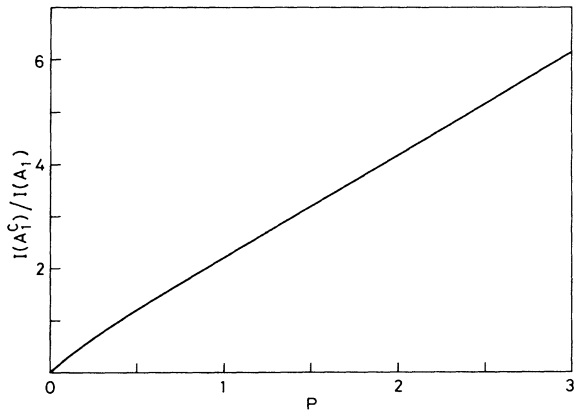

FIG. 17. The P dependence of the intensity ratio $I(A_1^c)/I(A_1)$ calculated from the stochastic RNM.

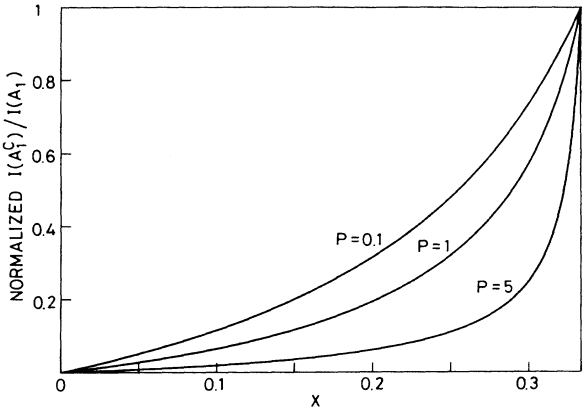

FIG. 18. The x dependence of the intensity ratio $I(A_1^c)/I(A_1)$.

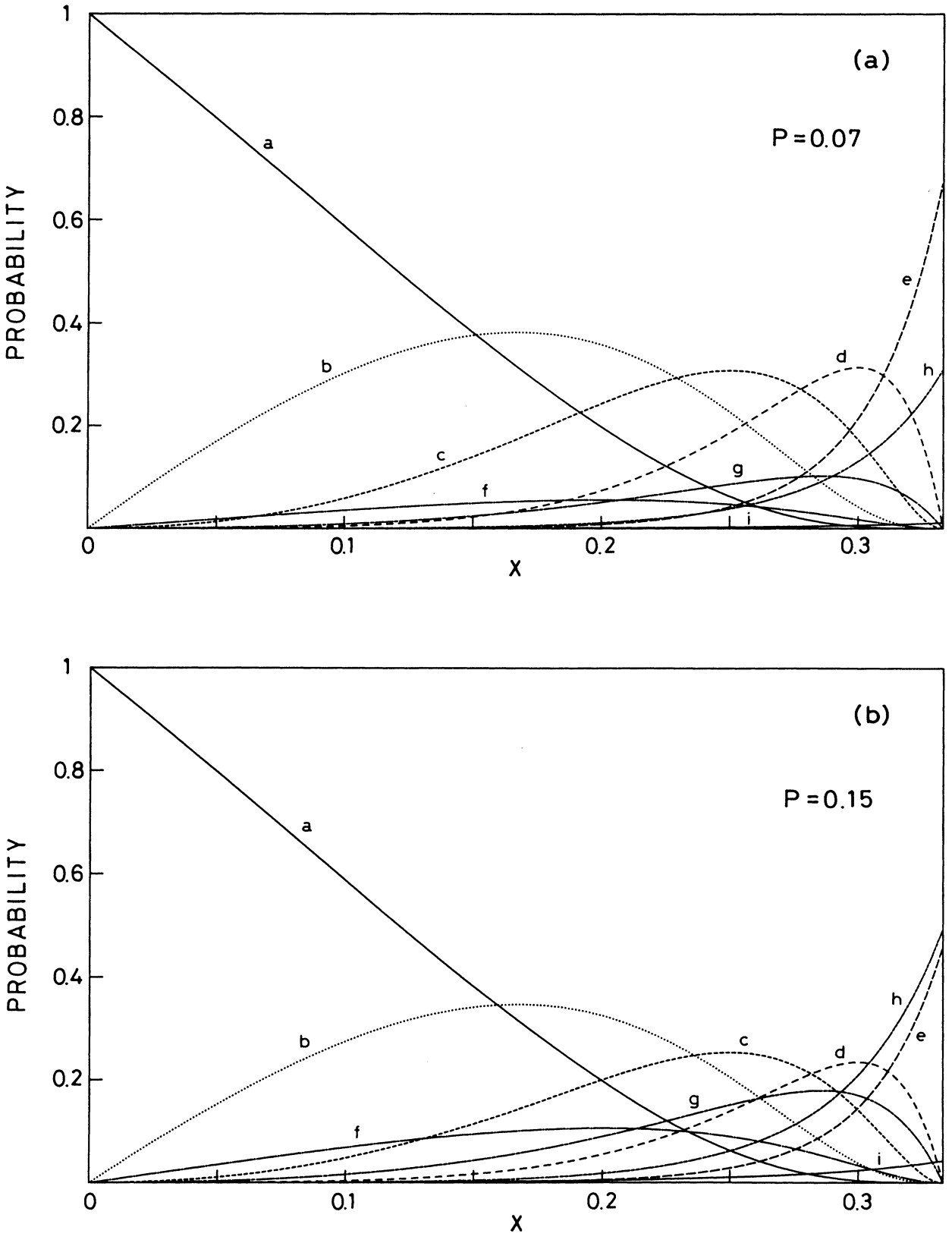

FIG. 19. The relative existing probability of the molecular bonding forms shown in Fig. 16 for $P = 0.07$, 0.15, and 2.2.

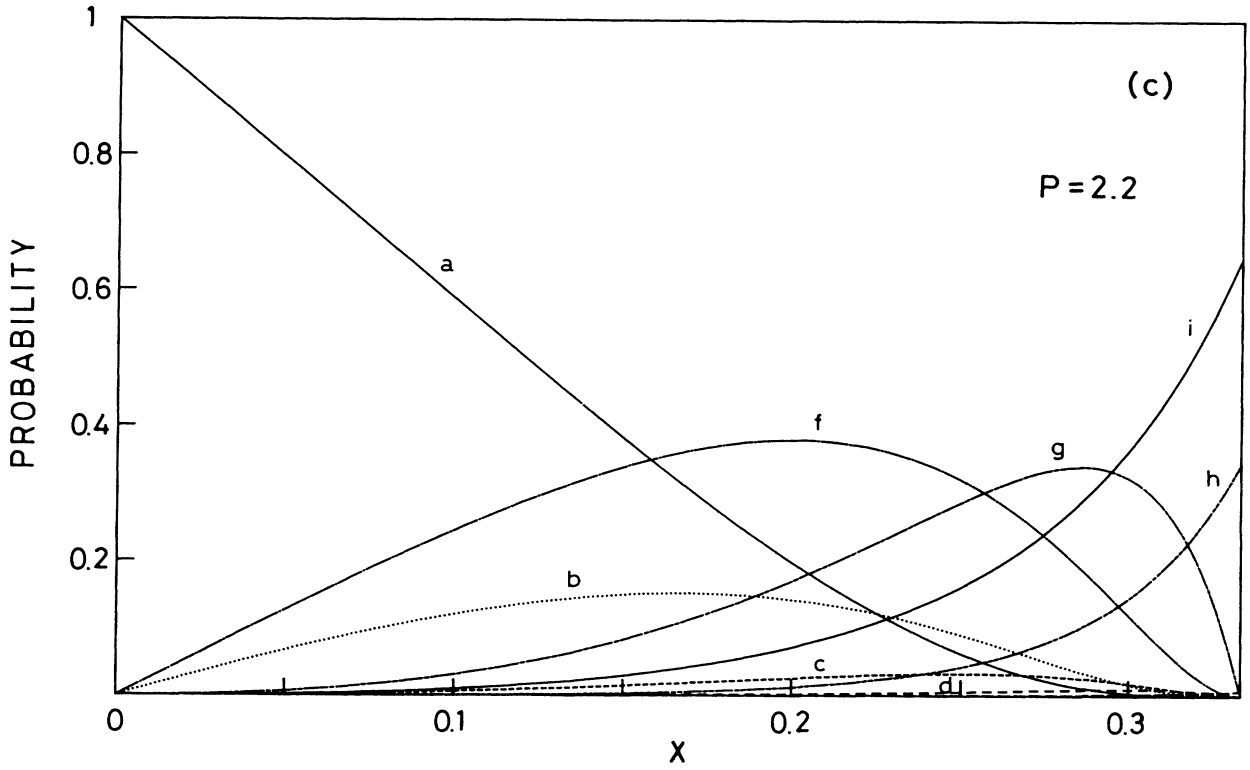

FIG. 19. (*Continued*).

$I(A_1^c)/I(A_1)$ in Ge_xSe_{1-x}, Ge_xS_{1-x}, and Si_xSe_{1-x} glasses are obtained with the adjustable parameter P which is independent of x. The obtained values are $P=0.15$ for Ge_xSe_{1-x}, $P=0.07$ for Ge_xS_{1-x}, and $P=2.2$ for Si_xSe_{1-x}. The x dependence of the intensity ratio is plotted using solid curves in Figs. 6, 10, and 14. The accordance with the experimental results is very good. The values of P can be obtained independently from the $I(A_1^c)/I(A_1)$ at $x=0.33$ with the assumption that the Raman scattering intensity is proportional to the number of chalcogen atoms irrespective of the modes in Figs. 2(a) and 2(b). These values are denoted by P^*. The obtained values of P^* are 0.15 for Ge_xSe_{1-x}, 0.07 for Ge_xS_{1-x}, and 1.44 for Si_xSe_{1-x}. It should be noticed that the values of P^* show small dependence on the incident laser wavelength. The obtained values are summarized in Table IV. The good coincidence between the values of P and P^* obtained from two different ways suggests the appropriateness of the present model.

In the crystals the corresponding P' is presented by the ratio of the number of chalcogen atoms on the edge-sharing (ES) double bonds to that on the corner-sharing (CS) bonds, $n(\mathrm{ES})/n(\mathrm{CS})$, from Fig. 17 by replacing $I(A_1^c)/I(A_1)$ with $n(\mathrm{ES})/n(\mathrm{CS})$ and P with P'. In the low-temperature (LT) phase of GeS_2, P' equals zero, since the structure is composed of only the corner-sharing bonds. In $GeSe_2$ and the high-temperature (HT) phase of GeS_2 the ratio $n(\mathrm{ES})/n(\mathrm{CS})$ is $\frac{1}{3}$, which corresponds to $P'=0.12$. In SiS_2 and $SiSe_2$, $P'=\infty$ since the crystal is formed of only the edge sharing bonds. These results are also listed in Table IV. The order of increasing P (P' and P^*) from Ge_xS_{1-x}, Ge_xSe_{1-x}, Si_xSe_{1-x} to Si_xS_{1-x} is the same in the glassy and the crystalline states. The large difference of the values of P (P' and P^*) between the glass and the crystal suggests that the glass is not constructed simply from the fragment of the crystal.

Figure 19 shows the relative existing probability of the molecular bonding forms shown in Fig. 16 for the values of P obtained from the best fit for the x dependence of $I(A_1^c)/I(A_1)$ in Ge_xS_{1-x}, Ge_xSe_{1-x}, and Si_xSe_{1-x}. The most probable bonding form changes with x. The probability of the form of Fig. 16(a) increases monotonically to one, when x approaches zero. The probability of the bonding forms of Figs. 16(e), 16(h), and 16(i) increases monotonically with the increase of x.

V. PHOTOINDUCED MICROCRYSTALLIZATION

The value of P is intrinsic in each disordered material and not affected by the method used in making the sample, but it can be changed by the irradiation of light. The Raman spectrum in amorphous $GeSe_2$ which is made by the vacuum evaporation method shows the same structure as that in the glass which is made by the melt-quenched method. This fact is difficult to explain within the ORM in which the companion peak is related to the boundary structure of the crystalline fragment because it is expected that the size of the fragment decreases with the increase of cooling speed.

Photoirradiation can, however, change the P. The irra-

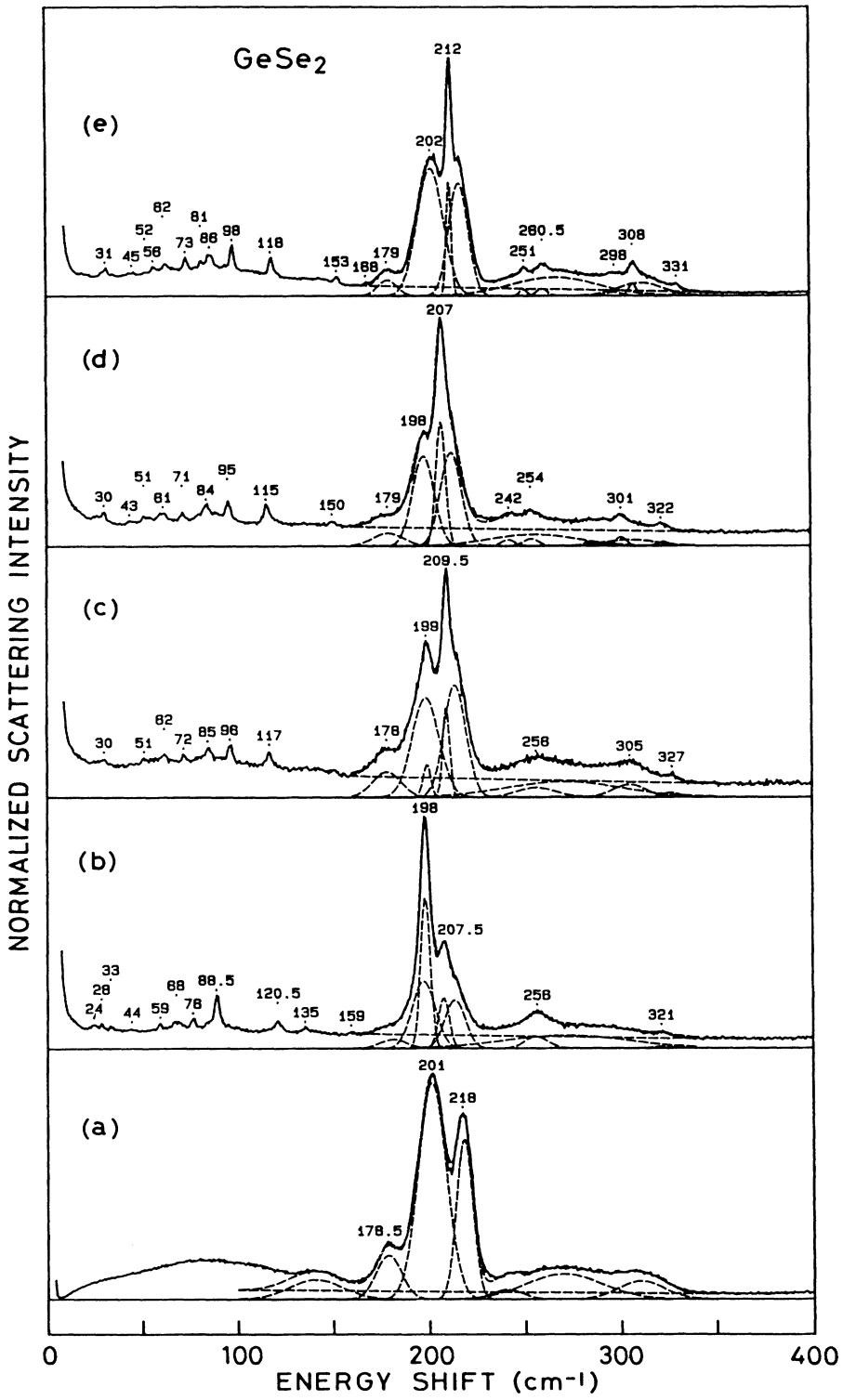

FIG. 20. The Raman spectra in the microcrystalline states of $GeSe_2$ induced by photoirradiation (b)—(d) and by thermal annealing (e). A 6328 Å laser beam was used. The spectrum in (a) is obtained from the glass before the crystallization. The spectrum in (b) was measured at the incident light power density of 0.6 kW/cm^2 after the irradiation with the same power density for 330 min. The spectra in (c) and (d) were measured at 0.4 kW/cm^2 and 0.8 kW/cm^2 after the irradiation of 0.8 kW/cm^2 for 840 min, respectively. The spectrum in (c) shows the microcrystalline state formed by the thermal annealing at 400 °C for 14 h.

diation of low-density light below the threshold increases the intensity of the A_1 peak, which corresponds to the increase of the corner-sharing bonds and the decrease of P in the present model, while high-density light increases the A_1^c peak, which corresponds to the increase of the edge-sharing bonds and the increase of P.

Figure 20 shows the spectral change due to the crystallization by photoirradiation [Figs. 20(b)—20(d)] as well as by thermal annealing [Fig. 20(e)]. The Gaussian decomposition curves are also shown. The data of the Gaussian fits are listed in Table V. The spectrum Fig. 20(a) is the typical one in the glass. The spectrum was obtained at the laser power of 15 mW with the use of a cylindrical lens of the focal length 10 cm. The incident light power density on the sample surface is estimated at 8 W/cm^2. The spectra in Figs. 20(b), 20(c), and 20(d) show the creation of microcrystals by photoirradiation. The measurement of Raman scattering and the photoirradiation for the crystallization were done at the same optical arrangement with the same laser beam, but with different intensity. A spherical convex lens with the focal length of 10 cm was used to focus the beam on the sample surface. The spectrum in Fig. 20(b) was obtained at the laser power of 12 mW after the photoirradiation with the same laser power for 330 min. The effective incident power density is estimated at 0.6 kW/cm^2. The spectrum in Fig. 20(c) was measured at 8 mW after the irradiation of 15 mW for 840 min. The spectrum in Fig. 20(d) was measured at 15 mW just after the scan [Fig. 20(c)]. The spectrum measured at 8 mW just after the scan [Fig. 20(d)] came back to the spectrum in Fig. 20(c). These photoinduced microcrystallization is irreversible, which is contrary to the results by Griffiths *et al.*[9] The spectrum in Fig. 20(e) was measured at 15 mW using a cylindrical lens on the sample annealed for 14 h at 400 °C which is just above the glass transition temperature 392 °C.[9]

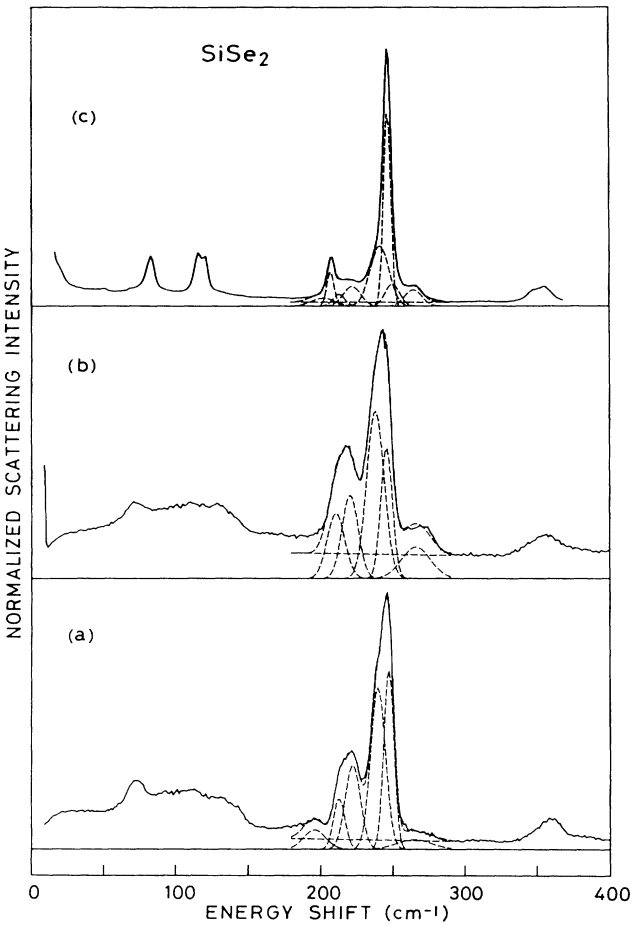

FIG. 21. The Raman spectra in the process of photoinduced microcrystallization in $SiSe_2$ glass. The measurement and the photoirradiation were made with a 4579 Å laser beam. The spectrum in (a) is obtained in the glass before the crystallization. The spectra in (b) and (c) were measured at 1.5 kW/cm^2 after the irradiation of 1.5 kW/cm^2 for 310 min and 3 kW/cm^2 for 10 min, respectively.

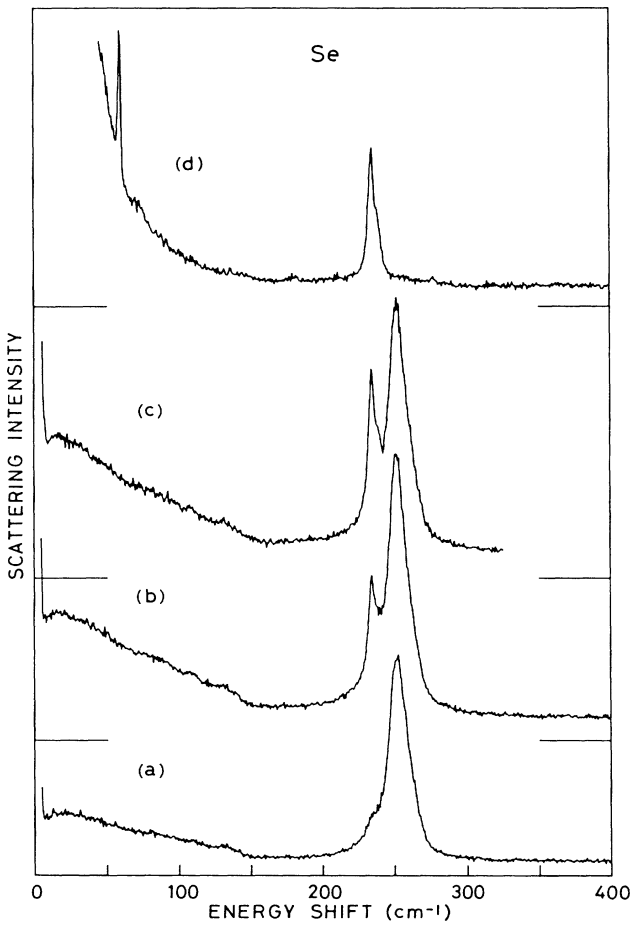

FIG. 22. The Raman spectra in the process of photoinduced structural change in Se glass. A 6328 Å laser beam was used. The spectrum in (a) is for Se glass, which was measured at 4 W/cm^2. The spectra in (b), (c), and (d) were measured at 8 W/cm^2, 8 W/cm^2, and 0.8 kW/cm^2 just after the start of the irradiation, respectively.

TABLE V. The phonon energies, scattering intensities normalized by the A_1 peak intensity and the standard deviations of the energies in the $GeSe_2$ glass and its microcrystallized states shown in Fig. 20. The A_1 mode is denoted by A, the A_1^c by C and the dominant crystalline mode by cr.

Spectrum	Mode	ω (cm^{-1})	I	σ (cm^{-1})
(a)		140.4	0.17	13.9
		178.5	0.18	6.5
	A	201.2	1.00	7.3
	C	218.0	0.43	4.2
		240.0	0.05	8.0
		269.5	0.32	20.0
		310.0	0.14	12.0
(b)		181.0	0.08	7.0
	A	197.0	0.52	6.0
	A,cr	198.0	0.48	2.5
	cr	207.5	0.18	2.8
	C	213.3	0.33	5.3
		255.5	0.09	6.0
		271.0	0.55	33.0
		321.0	0.01	5.5
(c)		178.3	0.24	7.3
	A	198.6	0.91	7.0
	A,cr	199.2	0.09	2.0
	cr	209.4	0.21	1.8
	C	213.9	0.84	5.7
		256.0	0.13	10.0
		270.0	0.61	30.0
		305.0	0.14	8.5
		327.0	0.02	4.0
(d)		179.5	0.20	8.0
	A	198.0	1.00	5.6
	cr	207.1	0.62	2.5
	C	212.4	1.00	5.4
		242.0	0.04	3.5
		254.0	0.06	4.0
		255.0	0.53	23.0
		285.0	0.03	3.0
		292.0	0.02	2.5
		301.0	0.05	3.0
		306.0	0.18	14.0
		323.0	0.03	3.0
(e)		179.7	0.09	5.0
	A	202.3	1.00	6.8
	cr	212.0	0.17	1.3
	C	217.0	0.65	5.0
		250.7	0.02	2.0
		260.5	0.02	2.8
		266.5	0.50	23.0
		298.0	0.02	4.0
		308.0	0.03	2.0
		312.0	0.18	12.0
		331.0	0.01	2.0

The spectra in Figs. 20(b)—20(e) are composed of the mixed structure of the glass and the crystal. There is an essential difference between the spectrum in Fig. 20(b) and the spectra in Figs. 20(c)—20(e). The energies of many sharp peaks which appear in the spectra in Figs. 20(c), 20(d), and 20(e) are essentially the same as in the crystal except for the peaks at 51, 199, and 327 cm^{-1}, although the strong irradiation shifts the peak energies to the lower-energy direction as shown in the spectrum in Fig. 20(d). The spectrum in Fig. 20(b), obtained after the irradiation below the threshold intensity, shows many sharp crystalline peaks the energies of which are different from the $GeSe_2$ crystal. This microcrystalline phase is assigned to the low-temperature phase of GeS_2.[29] The modes at 24, 28, 33, 44, 59, 68, 76, 88.5, 120.5, 135, 159, and 198 cm^{-1} are originated from this new microcrystalline phase.

The trials to synthesize the new phase of $GeSe_2$ from the thermal annealing of glassy $GeSe_2$ or a liquid-phase growth from excess Se liquid resulted in failure till now. This two-directional photoinduced crystallization is the first evidence, to the best of my knowledge, that the photoinduced microcrystallization is clearly distinguished from the thermal crystallization.

As a result of the photoirradiation the intensity ratio of the glassy peaks, $I(A_1^c)/I(A_1)$, changes drastically. The irradiation below the threshold intensity decreases the intensity ratio from 0.43 ($P^*=0.16$) to 0.33 ($P^*=0.12$), while the irradiation above it increases the ratio to 1 ($P^*=0.41$) as listed in Table V. The increase of $I(A_1^c)/I(A_1)$ is contrary to the experimental results by Griffiths *et al.*[9,32] They cited the simultaneous disappearance of the A_1^c peak and the 178 cm^{-1} peak which has

TABLE VI. The phonon energies, scattering intensities normalized by the A_1 peak intensity, and the standard deviations of the energies in the $SiSe_2$ glass and its microcrystallized states shown in Fig. 21. The A_1 mode is denoted by A, the A_1^c by C and the dominant crystalline mode by cr.

Spectrum	Mode	ω (cm^{-1})	I	σ (cm^{-1})
(a)		195.8	0.23	7.5
	A	212.8	0.31	3.9
	A	222.1	0.69	5.2
	C	239.5	1.29	5.1
	C	247.0	0.98	3.5
		264.5	0.18	12.0
(b)	A	210.7	0.46	6.0
	A	220.4	0.54	5.5
	C	237.9	1.18	6.0
	C	245.6	0.61	4.0
		266.0	0.37	10.0
(c)		202.0	0.39	8.0
	cr	207.2	0.51	2.5
	A	213.0	0.29	4.0
	A	222.0	0.71	6.0
	C	241.0	2.37	6.5
	cr	246.3	2.96	2.5
	C	250.0	0.67	5.0
		264.5	0.59	6.0

been assigned to the vibrational mode in the ethane-like molecules as the evidence of the validity of the ORM.

In the ORM the A_1^c mode is assigned to the vibration in the structure which does not exist in the crystal. In the course of photoinduced crystallization, the ORM predicts that the A_1 peak increases and shifts to the energy of the crystalline A_g peak at 211 cm^{-1} as well as the decrease of the A_1^c peak. This prediction is contrary to the experimental results that the crystalline peak sprouts at almost the same energy with the A_g peak in the $GeSe_2$ crystal and the A_1^c peak does not disappear.

The crystallization by the thermal annealing shows the saturated behavior to the level which is determined by the annealing temperature. The peak height strongly depends on the annealing temperature.

Photoinduced crystallization in $SiSe_2$ glass is shown in Fig. 21 together with the Gaussian curves. The data of the Gaussian decomposition are shown in Table VI. The Ar-ion laser was operated at 4579 Å in this experiment. The spectrum in Fig. 21(a) was measured before the crystallization at 3 mW (0.3 kW/cm^2). The spectra in Figs. 21(b) and 21(c) were measured at 15 mW after the irradiation of 15 mW for 310 min and 30 mW for 10 min, respectively. The relative intensity $I(A_1^c)/I(A_1)$ decreases from 2.3 ($P^*=1.05$) in the glass to 1.8 ($P^*=0.80$) by the weak light and increases to 3 ($P^*=1.41$) by the strong light.

This photoinduced crystallization shows that the local energy is lower in the corner-sharing bond than in the edge-sharing bond, but the total energy is lowest in the normal crystal structure. Therefore in the $GeSe_2$ glass the microcrystals with the low-temperature phase of GeS_2 are formed, when the molecules are excited independently, but the structure changes to the high-temperature phase of GeS_2, when all molecules are excited simultaneously. The minimum sizes of the microcrystals which give the crystalline spectra are speculated to the order of $10\times10\times10$ in the units of the lattice constants of the crystal. In the case of *a*-Si a recent high-resolution electron microscope elucidated the cluster structure.[42] Inside the cluster Si atoms are arranged as in the crystal. The number of atoms in a cluster is on the order of 1000. The Raman spectra from *a*-Si shows small crystalline peaks which are superimposed on the broad amorphous peak.

The threshold intensity for the crystallization in Se glass is less than $\frac{1}{100}$ of that in $GeSe_2$ glass. The threshold intensity increases rapidly with the increase of Ge or Si concentration. Figure 22 shows the photoinduced crystallization in Se glass. The spectrum in Fig. 22(a) was measured at the incident laser beam of 8 mW focused by a cylindrical lens with the focal length of 10 cm. The effective incident power is estimated to 4 W/cm^2. The spectra in Figs. 22(b) and 22(c) were successively measured at the laser power of 15 mW with the same lens without the special time of the photoinduced crystallization. The spectrum in Fig. 22(d) was obtained immediately after the photoirradiation of 15 mW with a spherical lens with the focal length of 10 cm. The effective incident power is estimated to 0.8 kW/cm^2. The peak at 251.5 cm^{-1} is assigned to the A_1 mode in the Se_8 rings and the 234 cm^{-1} peak to the A_1 mode in the polymeric chains.[40] This structural change is the same as that by thermal annealing.[43] A vector charge-density wave model was proposed for the amorphous structure of Se by Fukutome.[44] In his model the amorphous structure is characterized by the charged soliton caused by the defect in the spiral bonding structure. The crystallization may be caused by the excited soliton created by the irradiated light. The existence of the threshold intensity for the start of crystallization suggests that the cooperative phenomena of excited solitons is necessary for the crystallization.

VI. DISCUSSION

It is shown in the preceding section that the stochastic RNM which has only one parameter P can explain consistently the origin of the A_1 and the A_1^c peaks which have been the cause of the controversy about the amorphous structure. In this section the remaining problems are discussed.

Mössbauer spectroscopy by Bresser *et al.*[45] showed the existence of two chalcogen sites in $GeSe_2$ and GeS_2 glasses. They assigned one site to the Ge—Se—Ge bond and another site to the Ge—Se—Se bond. The second Se site was attributed to the dimerized chalcogen atoms on the edges of the outrigger-raft clusters. I suggest the possibility of assignment that the second site can be attributed to the edge-sharing bond because the interatomic distance between the chalcogen atoms is shorter than twice the ionic radius.[35] Some covalent bonding force is expected between the two chalcogen atoms.

The structure of glass in the RNM is essentially three dimensional, while the structure in the ORM is two dimensional. The low-frequency peak at about 22 cm^{-1} in the Raman spectra, which is often called the Bose peak, is explained by the rigid layer mode in the ORM.[6] The rigid layer mode is a characteristic mode in two-dimensional materials. However, as shown in Figs. 3, 7, 11, and 15 this peak is observed, only if the surface is good, in SiS_2 and Si_xSe_{1-x} with one-dimensional crystal structure, in Ge_xSe_{1-x} with two-dimensional crystal structure, and in Ge_xS_{1-x} with two- and three-dimensional crystal structures, and even in Se with one-dimensional and ring structures. The Bose peak is commonly observed in many amorphous materials.[46] Martin and Brenig[47] explained the Bose peak as fluctuation of the polarizability by the acoustic wave. Nemanich[46] and Arai *et al.*[48] used this model for the analysis of the Bose peak in As_2S_3. Recent theory of phonon localization by Akkermans *et al.*[33] shows that the spectral density is enhanced near the frequency of phonon localization.

The present experimental results of Raman scattering are consistent with the present stochastic random network model. It should be stressed again that this model is based on the interpretation of the Raman spectra from the viewpoint of phonon localization. When regular structure extends to several or several tens of the crystalline lattice constant in each direction, the coherent crystalline mode appears. This mode extends to the whole cluster and has the energy of the crystalline A_g mode. Further advances are highly expected in the theoretical works which solve the localization-delocalization problem of phonons.

ACKNOWLEDGMENTS

The computer program SALS written by T. Nakagawa and Y. Koyanagi and co-workers was used in the calculation of the least-squares fitting. The present work is supported by the Nippon Sheet Glass Foundation for Materials Science.

[1]P. Tronc, M. Bensoussan, A. Brenac, and C. Sebenne, Phys. Rev. B **8**, 5947 (1973).
[2]R. J. Nemanich, S. A. Solin, and G. Lucovsky, Solid State Commun. **21**, 273 (1977).
[3]N. Kumagai, J. Shirafuji, and Y. Inuishi, J. Phys. Soc. Jpn. **42**, 1262 (1977).
[4]R. J. Nemanich, G. A. N. Connell, T. M. Hayes, and R. A. Street, Phys. Rev. B **18**, 6900 (1978).
[5]H. Kawamura and M. Matsumura, Solid State Commun. **32**, 83 (1979).
[6]P. M. Bridenbaugh, G. P. Espinosa, J. E. Griffiths, J. C. Phillips, and J. P. Remeika, Phys. Rev. B **20**, 4140 (1979).
[7]H. Kawamura, M. Matsumura, and S. Ushioda, J. Non-Cryst. Solids **35& 36**, 1215 (1980).
[8]J. E. Griffiths, G. P. Espinosa, J. P. Remeika, and J. C. Phillips, Solid State Commun. **40**, 1077 (1981).
[9]J. E. Griffiths, G. P. Espinosa, J. P. Remeika, and J. C. Phillips, Phys. Rev. B **25**, 1272 (1982).
[10]J. E. Griffiths, J. C. Phillips, G. P. Espinosa, and J. P. Remeika, Phys. Rev. B **26**, 3499 (1982).
[11]T. Fukunaga, Y. Tanaka, and K. Murase, Solid State Commun. **42**, 513 (1982).
[12]J. E. Griffiths, G. P. Espinosa, J. C. Phillips, and J. P. Remeika, Phys. Rev. B **28**, 4444 (1983).
[13]M. Balkanski, E. Haro, G. P. Espinosa, and J. C. Phillips, Solid State Commun. **51**, 639 (1984).
[14]M. Stevens, P. Boolchand, and J. G. Hernandez, Phys. Rev. B **31**, 981 (1985).
[15]E. Haro, Z. S. Xu, J.-F. Morhange, M. Balkanski, G. P. Espinosa, and J. C. Phillips, Phys. Rev. B **32**, 969 (1985).
[16]G. Lucovsky, J. P. deNeufville, and F. L. Galeener, Phys. Rev. B **9**, 1591 (1974).
[17]G. Lucovsky, F. L. Galeener, R. C. Keezer, R. H. Geils, and H. A. Six, Phys. Rev. B **10**, 5134 (1974).
[18]R. J. Nemanich, M. Gorman, and S. A. Solin, Solid State Commun. **21**, 277 (1977).
[19]B. A. Weinstein, R. Zallen, M. L. Slade, and J. C. Mikkelsen, Jr., Phys. Rev. B **25**, 781 (1982).
[20]K. Arai, J. Non-Cryst. Solids **59& 60**, 1059 (1983).
[21]M. Tenhover, M. A. Hazle, and R. K. Grasselli, Phys. Rev. Lett. **51**, 404 (1983).
[22]M. Tenhover, M. A. Hazle, R. K. Grasselli, and C. W. Tompson, Phys. Rev. B **28**, 4608 (1983).
[23]M. Tenhover, M. A. Hazle and R. K. Grasselli, Phys. Rev. B **28**, 5897 (1983).
[24]M. Tenhover, R. S. Henderson, D. Lukco, M. A. Hazle, and R. K. Grasselli, Solid State Commun. **51**, 455 (1984).
[25]J. E. Griffiths, M. Malyj, G. P. Espinosa, and J. P. Remeika, Phys. Rev. B **30**, 6978 (1984).
[26]J. E. Griffiths, M. Malyj, G. P. Espinosa, and J. P. Remeika, Solid State Commun. **53**, 587 (1985).
[27]M. Malyj, G. P. Espinosa, and J. E. Griffiths, Phys. Rev. B **31**, 3672 (1985).
[28]M. Tenhover, M. A. Hazle, and R. K. Grasselli, J. Phys. C **18**, 2025 (1985).
[29]S. Sugai, Phys. Rev. Lett. **57**, 456 (1986).
[30]R. J. Nemanich, F. L. Galeener, J. C. Mikkelsen, Jr., G. A. N. Connell, G. Etherington, A. C. Wright, and R. N. Sinclair, Physica **117& 118B**, 959 (1983).
[31]G. Lucovsky, C. K. Wong, and W. B. Pollard, J. Non-Cryst. Solids **59& 60**, 839 (1983).
[32]J. E. Griffiths, J. C. Phillips, G. P. Espinosa, J. P. Remeika, and P. M. Bridenbaugh Phys. Status Solidi B **122**, K11 (1984).
[33]E. Akkermans and R. Maynard, Phys. Rev. B **32**, 7850 (1985).
[34]Von G. Dittmar and H. Schäfer, Acta Cryst. B **32**, 1188 (1976).
[35]Von G. Dittmar and H. Schäfer, Acta Cryst. B **32**, 2726 (1976).
[36]Von G. Dittmar and H. Schäfer, Acta Cryst. B **31**, 2060 (1975).
[37]J. Peters and B. Krebs, Acta Cryst. B **38**, 1270 (1982).
[38]K. Murase, T. Fukunaga, Y. Tanaka, K. Yakushiji, and I. Yunoki, Physica **117& 118B**, 962 (1983).
[39]J. A. Aronovitz, J. R. Banavar, M. A. Marcus, and J. C. Phillips, Phys. Rev. B **28**, 4454 (1983).
[40]G. Lucovsky, A. Mooradian, W. Taylor, G. B. Wright, and R. C. Keezer, Solid State Commun. **5**, 113 (1967).
[41]D. W. Scott, J. P. McCullough, and F. H. Kruse, J. Mol. Spectrosc. **13**, 313 (1964).
[42]A. Chenevas-Paule and A. Bourret, J. Non-Cryst. Solids **59& 60**, 233 (1983).
[43]G. Carini, M. Cutroni, G. Galli, P. Migliardo, and F. Wanderlingh, Solid State Commun. **33**, 1139 (1980).
[44]H. Fukutome, Prog. Theor. Phys. **71**, 1 (1984).
[45]W. J. Bresser, P. Boolchand, P. Suranyi, and J. P. de Neufville, Phys. Rev. Lett. **46**, 1689 (1981).
[46]R. J. Nemanich, Phys. Rev. B **16**, 1655 (1977).
[47]A. J. Martin and W. Brenig, Phys. Status Solidi B **64**, 163 (1974).
[48]T. Arai, H. Kataura, H. Yasuoka, and S. Onari, J. Non-Cryst. Solids **77& 78**, 1149 (1985).